Si(^{3}P) + OH($X^2\Pi$) Interaction: Long-Range Multipolar Potentials of the Eighteen Spin−Orbit States†

Béatrice Bussery-Honvault*

Institut UTINAM, UMR CNRS 6213, Université de Franche-Comté, 25030 Besançon cedex, France

Fabrice Dayou

LERMA, UMR 8112, Observatoire de Paris-Meudon, 92195 Meudon cedex, France

Received: May 30, 2009; Revised Manuscript Received: September 2, 2009

Eighteen spin−orbit states are generated from the open-shell open-shell Si(^{3}P) + OH($X^2\Pi$) interacting system. We present here the behavior of the associated long-range intermolecular potentials, following a multipolar expansion of the Coulombic interaction treated up to second order of the perturbation theory, giving rise to a series of terms varying in R^{-n}. In the present work, we have considered the electrostatic dipole−quadrupole ($n = 4$) and quadrupole−quadrupole ($n = 5$) interactions, as well as the dipole−induced dipole−induced dispersion ($n = 6$) and dipole−dipole-induced induction ($n = 6$) contributions. The diatomic OH is kept fixed at its ground state-averaged distance, $(r)_{v=0} = 1.865$ bohr, so that the long-range potentials are two-dimensional potential energy surfaces (PESs) that depend on the intermolecular distance R and on the bending angle $\gamma = \angle$SiGH, where G represents the mass center of OH. From the calculated properties of the monomers, such as the dipole and quadrupole moments and static and dynamic polarizabilities, we have determined and tabulated the long-range coefficients of the multipolar expansion of the potentials for each matrix elements. The isolated monomer spin−orbit splittings have been included in the final matrix, whose diagonalization gives rise to 18 adiabatic potentials. Then, the adiabatic states have been compared to potential energies given by supermolecular ab initio calculations resulting in a general good overall agreement.

I. Introduction

Studies of the reactions that lead to the formation of SiO molecules are necessary to understand the interstellar chemistry of silicon. The SiO molecule is largely observed in molecular outglows surrounding stars during their formation, and it is used as a spectroscopic probe of shocked regions.[1,2] Models suggest that the interstellar production of gas phase SiO occurs via reactions of ground state silicon, which is released from grain cores by local shocks, with either O_2 or OH radicals.[3,4] But while the reaction between Si and O_2 has been studied both experimentally[4,5] and theoretically,[6,7] there exist no comparable studies of the formation reaction of SiO from Si and OH. The latter reaction is relevant to the characterization of SiO formation processes occurring at temperatures corresponding to the warm shocked layers (on the order of 100 K) and the cool postshock flow (on the order of 10 K). The Si + OH reaction is also relevant to the formation of the HSiO−SiOH isomeric system,[8] which is the third-row analog of the HCO−COH system that we have previously examined.[9−13] Both of the isomers are possible reactive intermediates in chemical vapor deposition processes and plausible candidates for astronomical detection (as has been the case of HCO[14]).

Experiments involving two radical species have proven to be difficult to perform,[15−18] particularly in the low temperature range relevant to interstellar chemistry. A theoretical approach obviates the experimental difficulties and is well-suited to modeling the reaction at low temperature. The low temperature condition limits reactions to those that occur without a potential barrier for the optimal angle of approach, and this is hopefully the case for most radical−radical collisions. In such scenarios it is important that the long-range part of the potential energy surfaces be accurately described since it is this part that governs the reactivity at low temperature. Here is the purpose of this paper. At large separations, the overlap of the wave functions corresponding to the two interacting species can be neglected. The interaction potential operator can therefore be written as a multipole expansion, which leads to potential matrix elements that are expressed in terms of inverse powers of the intermolecular distance R. The coefficients of such an expansion are then valuable quantities for accurately predicting the asymptotic behavior of the potentials. The general approach, however, is complicated by the fact that the Si(^{3}P) + OH($X^2\Pi$) system consists of two radicals and in such systems a large number of states arise from the interaction between degenerate species. This situation was encountered previously with the isoelectronic C(^{3}P) + OH($X^2\Pi$) system,[9] in which 18 states arise from the interaction when one includes relativistic effects, or 12 states if one neglects the spin−orbit fine structure. The fine structure splittings, however, can greatly influence the reaction kinetics because transitions may occur among the multiple states, and the behavior of the potentials differs markedly from the nonrelativistic case. In general, the initial states populations are presumed to partition adiabatically onto reactive and nonreactive surfaces. The spin−orbit contribution is included through an electronic partition factor that accounts for the relative population of the reactive states,[6,11,19] but this approach assumes that the potential remains unchanged from the nonrelativistic case. In this paper we seek to address the problem of accurately

† Part of the "Vincenzo Aquilanti Festschrift".

* Author to whom correspondence should be addressed. E-mail: beatrice.honvault-bussery@univ-fcomte.fr.

10.1021/jp905090x
Published on Web 09/25/2009

describing the long-range potentials by first presenting the behavior of the 12 potentials resulting from the Si(^{3}P) + OH($X^2\Pi$) interaction. We next demonstrate how these long-range potentials give rise to 18 relativistic states when the spin−orbit interaction is included.

After a brief introduction of the theoretical model, we present in section III the evaluation of the monomer properties that are used in the calculation of the long-range coefficients whose numerical values are given in section IV. We discuss in section V the behavior of the long-range potentials with or without inclusion of the spin−orbit splittings.

II. Theoretical Model

The long-range potentials are described by the perturbation theory up to second order by using a two-center expansion of the intermolecular Coulombic potential. For calculations describing interactions over large intermolecular distances, a multipolar expansion of the Coulombic operator, as given by eq 1 of ref 9, can be used in good approximation, resulting in potential energies represented by a series of terms varying in R^{-n}. The first-order perturbation yields electrostatic energies that include the permanent multipole moments of the monomers, which in the present case is described by the quadrupole−dipole and quadrupole−quadrupole interactions only, and the resultant potential matrix elements vary as R^{-4} and R^{-5}, respectively. The second-order perturbation gives rise to the dispersion and the induction energies involving induced multipole moments, and this is truncated to terms in R^{-6}. Since the long-range interactions are determined by intrinsic properties of each monomer, such as the permanent multipole moments and static and dynamic polarizabilities, these quantities must be evaluated with a good accuracy. To describe the long-range part of such an atom−diatom system, we employed the usual set of Jacobi coordinates, i.e., the intermolecular separation R between the silicon atom and the OH center-of-mass, the OH internuclear distance r, and the angle γ between the two vectors R and r, where $\gamma = 0°$ corresponds to linear OHSi and $\gamma = 180°$ to linear SiOH. The OH internuclear distance r has been kept fixed at its ground vibrational state averaged distance $(r)_{v=0} = 1.865$ a_0, and, thus, we are actually dealing with two-dimensional PESs matrix elements, depending on R and γ only. The formalism employed to evaluate the electrostatic, induction, and dispersion energies for the interaction between an open-shell atom and an open-shell diatomic has already been described in ref 9 and will not be repeated here. Furthermore, as the ground state silicon atom Si(^{3}P) is isoelectronic to the ground state carbon atom C(^{3}P), the use of the latter formalism for the Si + OH case will not differ from the C + OH case treated in ref 9.

For the electrostatic energy, eq 5 of ref 9 is used to evaluate the long-range coefficients in the uncoupled basis, and eq 4 to evaluate those coefficients in the coupled basis. In present work, we have considered the dipole−quadrupole and quadrupole−quadrupole interactions only in the electrostatic energy. In such a case, the electrostatic energy relies on the knowledge of the dipole and quadrupole moments of OH, and of the quadrupole moment of Si. Expressions for the dispersion long-range coefficients are given in eqs 8 and 9 of ref 9 in the coupled and uncoupled basis, respectively, and in eqs 11 and 12 for the induction long-range coefficients. In the present work, we have considered the dipole−induced dipole−induced interactions only in the dispersion energy, and the dipole−dipole-induced contribution only in the induction energy. The evaluation of the long-range coefficients thus relies on the knowledge of the dynamic dipole polarizabilities of Si and OH for the dispersion contribution, and on the knowledge of the dipole moment of OH and of the static dipole polarizabilities of Si for the induction contribution.

TABLE 1: Static Multipole Moments (in au) for Si(^{3}P) and OH($X^2\Pi$)

	Si(^{3}P)	OH($X^2\Pi$)
Q_1^0		0.6563,[a] 0.64628[b]
		0.651,[c,d] 0.6545,[e] 0.6512[f]
Q_2^0	3.3245,[a] 3.34[g]	1.3136,[a] 1.30827[b]
	3.691,[h] 3.297[i]	1.35,[c] 1.3939[e]
$Q_2^{\pm 2}$		−1.2528,[a] −1.21539[b,j]
		−1.070,[c] −1.1825[e]

[a] Present work. For OH, calculations are done at the mean geometry $(r)_{v=0} = 1.865$ a_0. [b] SE-MRCI-ACPF values of ref 22 for $(r)_{v=0} = 1.865$ a_0. [c] Reference 19. [d] Experimental value of ref 21. [e] MRCI values of ref 23 for $r_{OH} = 1.95$ a_0. [f] Experimental value of ref 24. [g] CCSD(T) value of ref 25. [h] RHF (small CASSCF) value of ref 26. [i] CASSCF value of ref 26. [j] Following eq 1, the $Q_2^{\pm 2}$ value of ref 22 has been multiplied by $\sqrt{2}$.

III. Permanent Multipole Moments and Static and Dynamic Polarizabilities

To estimate error bars on the long-range interaction coefficients calculated in the present work, we have used two different sets of values for the monomers properties that are required to evaluate these coefficients: the dipole moment of OH and, for Si and OH, the quadrupole moments and the static and dynamic dipole polarizabilities. The first set (called set A) includes our presently calculated values by means of the Dalton ab initio quantum chemistry code[20] and the following computational scheme.

The permanent multipole moments of Si and OH have been calculated as the expectation values of Cartesian multipole moment operators with CASSCF electronic wave functions. The CASSCF wave functions were generated by distributing four electrons among 13 orbitals (3s, 3p, 3d, 4s, and 4p) for Si, and 7 electrons among 9 orbitals ($2-6\sigma$ and $1-2\pi$) for OH. The inner-shell orbitals (1s, 2s, and 2p for Si, 1σ for OH) were kept frozen in their form obtained from ROHF calculations. The aug-cc-pVQZ and aug-cc-pV5Z atomic basis sets were employed for Si and OH, respectively. From this scheme, we obtained matrix elements of the electric dipole operator μ_z and traceless quadrupole moments Θ_{uu}, with $u = \{x, y, z\}$, for each atomic and molecular substate of definite symmetry (within the D_{2h} and C_{2v} point groups for Si and OH, respectively). Hereafter, these states are labeled $||M_L|^{\pm}\rangle$ for Si and $||\Lambda|^{\pm}\rangle$ for OH, where $\pm$ stands for the symmetry of the electronic wave function with respect to σ_{xz}, the reflection through the xz plane. We report in Table 1 the permanent multipole moments obtained for Si and OH together with other literature values. The values of Table 1 correspond to matrix elements of the spherical multipole moment operators Q_{lm} in the basis sets $|M_L = 0, \pm 1\rangle$ for Si(^{3}P) and $|\Lambda = \pm 1\rangle$ for OH($X^2\Pi$), which are the values required to evaluate the interaction coefficients. For Si, we report the quadrupole moment matrix element $Q_{20} \equiv (0|Q_{20}|0\rangle$. This is the unique independent component and the other nonzero matrix elements $\langle M_L|Q_{lm}|M'_L\rangle$ are easily obtained by means of the Wigner−Eckart theorem. For OH, we report the matrix elements of the dipole moment $Q_{10} \equiv \langle \pm 1|Q_{10}|\pm 1\rangle$ and quadrupole moments $Q_{20} \equiv \langle \pm 1|Q_{20}|\pm 1\rangle$ and $Q_{2\pm 2} \equiv \langle \pm 1|Q_{2\pm 2}|\mp 1\rangle$, which are the only nonzero matrix elements.

TABLE 2: Static Dipole Polarizabilities (in a_0^3) for Si(^{3}P) and OH(X$^2\Pi$)

Si(^{3}P)				OH(X$^2\Pi$)				
α_{zz}	α_{xx}	$\bar{\alpha}$	$\Delta\alpha$	$^{xx}\alpha_{zz}$	$^{xx}\alpha_{xx}$	$^{xx}\alpha_{yy}$	$\bar{\alpha}$	$\Delta\alpha$
31.936[a]	40.358[a]	37.55[a]	−8.42[a]	8.699[a]	6.258[a]	7.620[a]	7.525[a]	1.760[a]
31.83[b]	40.40[b]	37.54[b]	−8.57[b]	8.751[c]	6.374[c]	7.554[c]	7.560[c]	1.787[c]
31.56[d]	39.97[d]	37.17[d]	−8.41[d]				7.053[e]	
31.83[f]	40.17[f]	37.40[f]	−8.34[f]					
30.74[g]	39.44[g]	36.54[g]	−8.7[g]					

[a] Linear response values of present work. For OH, calculations are done at the mean geometry $(r)_{v=0} = 1.865\ a_0$. [b] CCSD(T) values of ref 29. [c] SE-MRCI-ACPF values of ref 22 for $(r)_{v=0} = 1.865\ a_0$. [d] CCSD(T) values of ref 30. [e] TDUHF values of ref 31 at $r_{OH} = 1.95\ a_0$. [f] CCSD(T) values of ref 32. [g] CASPT2 values of ref 26.

TABLE 3: Dynamic Dipole Polarizabilities (in a_0^3) for Si(^{3}P) and OH(X$^2\Pi$) and Specific Imaginary Frequency

Si(^{3}P)			OH(X$^2\Pi$)		
ω	$\alpha_{zz}{}^a$	$\alpha_{xx}{}^a$	$^{xx}\alpha_{zz}{}^a/^{xx}\alpha_{zz}{}^b$	$^{xx}\alpha_{xx}{}^a/^{xx}\alpha_{xx}{}^b$	$^{xx}\alpha_{yy}{}^a/^{xx}\alpha_{yy}{}^b$
0.0	31.936	40.358	8.699/8.751	6.258/6.374	7.620/7.554
0.1	28.940	35.009	8.469/8.509	6.074/6.181	7.350/7.267
0.2	22.795	25.743	7.865/7.875	5.680/5.720	6.704/6.579
0.3	17.048	18.349	7.065/7.045	5.200/5.179	5.942/5.787
0.4	12.720	13.301	6.230/6.191	4.694/4.664	5.212/5.062
0.5	9.650	9.918	5.449/5.408	4.205/4.200	4.563/4.448
1.0	3.321	3.328	2.869/2.886	2.424/2.512	2.495/2.527
1.5	1.646	1.644	1.705/1.724	1.515/1.554	1.539/1.558
2.0	0.995	0.990	1.120/1.120	1.022/1.018	1.038/1.024
2.5	0.676	0.667	0.790/0.775	0.730/0.706	0.744/0.712
3.0	0.494	0.483	0.586/0.564	0.544/0.513	0.558/0.520
4.0	0.303	0.288	0.357/0.334	0.332/0.303	0.345/0.308
5.0	0.208	0.191	0.240/0.219	0.222/0.199	0.233/0.202

[a] Linear response values of present work (see text). For OH, calculations are done at the mean geometry $(r)_{v=0} = 1.865\ a_0$. [b] SE-MRCI-ACPF values of ref 22 for $(r)_{v=0} = 1.865\ a_0$.

The latter matrix elements relate with the calculated expectation values of the Cartesian multipole moment operators as follows:

$$\begin{aligned}
&\langle \pm 1|Q_{10}|\pm 1\rangle = \langle x|Q_{10}^{+}|x\rangle = \langle x|\mu_z|x\rangle \\
&\langle \pm 1|Q_{20}|\pm 1\rangle = \langle x|Q_{20}^{+}|x\rangle = \langle x|\Theta_{zz}|x\rangle \\
&\langle \pm 1|Q_{2\pm 2}|\mp 1\rangle = -\sqrt{2}\langle x|Q_{22}^{+}|x\rangle = \\
&\quad -\sqrt{\frac{2}{3}}[\langle x|\Theta_{xx}|x\rangle - \langle x|\Theta_{yy}|x\rangle]
\end{aligned} \tag{1}$$

where $Q_{l|m|}^{\pm}$ are the real components of the multipole moments, and $|x\rangle = |1^+\rangle$ labels the OH(X$^2\Pi$) electronic wave function of $p = +1$ parity with respect to σ_{xz}.

The static and dynamic dipole polarizabilities of Si and OH have been calculated by means of the linear response method[27] based on the CASSCF wave functions previously defined. For each atomic and molecular substate of definite symmetry, the use of the linear response method provides a set of Cauchy moments, each of which corresponding to a given Cartesian component of the electric dipole operator μ_u, with $u = \{x, y, z\}$. We next use analytical continuation techniques following the $[n, n-1]_\alpha$ and $[n, n-1]_\beta$ Padé approximants procedures defined in ref 28 to get lower and upper bounds to the dynamic polarizabilities $^{vv}\alpha_{uu}(i\omega)$, where v stands for $||M_L|^{\pm}\rangle$ for Si and $||\Lambda|^{\pm}\rangle$ for OH. The use of $[n, n-1]_\alpha$ and $[n, n-1]_\beta$ Padé approximants led to a fast convergence of the self-dispersion coefficients $C_6 = 3/\pi\int_0^\infty {}^{vv}\alpha_{uu}(i\omega)\,{}^{vv}\alpha_{uu}(i\omega)\,d\omega$. These self-dispersion coefficients were computed by means of a Gauss−Legendre quadrature, using the $\omega_j = (\omega_{max}/2)(x_j + 1)$ change of variables to transform the $[0, \omega_{max}]$ interval into the suitable $[-1, +1]$ interval for the N-point Gauss−Legendre abscissas $x_{j=1,N}$. The value of ω_{max} is chosen sufficiently large such as $\alpha(i\omega_{max}) \approx 0$. With $n = 4$ for Si and $n = 6$ for OH, the C_6 coefficients corresponding to the lower and upper bounds of the dynamic polarizabilities are already converged to within less than 1%. We used as final results the dynamic polarizabilities $^{vv}\alpha_{uu}(i\omega)$ yielded by Padé approximants with $n = 8$ for Si and $n = 9$ for OH, for which the dispersion coefficients are converged within less than 0.05% for Si and $u = \{x, y, z\}$, and for OH within 0.03% for $u = \{z\}$, and 0.4% for $u = \{x, y\}$. We report in Tables 2 and 3 the static and dynamic polarizabilities at selected values of the imaginary frequency for Si and OH, together with other literature values. The values correspond to the Cartesian components $^{vv}\alpha_{uu}(i\omega)$ associated with a given substate v of definite symmetry, $|0^-\rangle$ for Si (^{3}P) and $|x\rangle = |1^+\rangle$ for OH (X$^2\Pi$). In the present case, for symmetry reasons, this limited set of Cartesian components of the polarizability is sufficient to get the whole set of spherical components $^{M_L M_L'}\alpha_{lml'm'}$ and $^{\Lambda\Lambda'}\alpha_{lml'm'}$ required to determine the interaction coefficients. For Si, the procedure used to derive the spherical components $^{M_L M_L'}\alpha_{lml'm'}$ from Cartesian ones is fully equivalent to that already proposed in ref 9. For OH, we know that the real components of the multipole moment satisfy $Q_{10}^{+} = \mu_z$, $Q_{11}^{+} = \mu_x$, and $Q_{11}^{-} = \mu_y$. Hence, the dipole polarizabilities corresponding to multipole moments $Q_{l|m|}^{\pm}$ and wave functions $||\Lambda|^{\pm}\rangle$ of definite symmetry are directly related to the Cartesian components, such as $^{xx}\alpha_{1010}^{++} = {}^{xx}\alpha_{zz}$, $^{xx}\alpha_{111}^{++} = {}^{xx}\alpha_{xx}$, and $^{xx}\alpha_{111}^{--} = {}^{xx}\alpha_{yy}$ for the $|x\rangle$ state. Using the usual relations between the spherical and real components of the multipole moments, Q_{lm} and $Q_{l|m|}^{\pm}$, and OH (X$^2\Pi$) wave functions, $|\pm 1\rangle$ and $|1^{\pm}\rangle$, one obtains the nonzero components of spherical dipole polarizabilities (see eq 11 of ref 9's EPAPS):

$$
\begin{aligned}
{}^{\pm 1 \pm 1}\alpha_{1010} &= {}^{xx}\alpha_{zz} \\
{}^{\pm 1 \pm 1}\alpha_{1\pm 11\mp 1} &= -\frac{1}{2}[{}^{xx}\alpha_{xx} + {}^{xx}\alpha_{yy}] = {}^{\pm 1 \pm 1}\alpha_{1\mp 11\pm 1} \\
{}^{\pm 1 \mp 1}\alpha_{1\pm 11\pm 1} &= -[{}^{xx}\alpha_{xx} - {}^{xx}\alpha_{yy}]
\end{aligned} \tag{2}
$$

where ${}^{xx}\alpha_{zz}$, ${}^{xx}\alpha_{xx}$, and ${}^{xx}\alpha_{yy}$ are the values reported in Tables 2 and 3.

As can be seen in Tables 1−3, our calculated values of the monomers properties lie in good agreement with most of the literature values. The relative discrepancies are less than 1% with the most recent ab initio values of the quadrupole moment Q_{20}^{Si} and static polarizabilities α_{uu}^{Si} of Si, of the dipole moment Q_{10}^{OH}, quadrupole moment Q_{20}^{OH}, and static polarizabilities α_{uu}^{OH} of OH. A spread of 2% is noticed with the $Q_{2\pm 2}^{OH}$ values of OH if fixed at $r_{v=0} = 1.865$ bohr. The larger discrepancies (up to 6%) observed for the quadrupole moments Q_{20}^{OH} and $Q_{2\pm 2}^{OH}$ of OH result from the use of different OH intradiatomic distances. For the dynamic polarizabilities $\alpha_{uu}^{OH}(i\omega)$ of OH with $u = \{x, y, z\}$, literature values lie within 7−9% on average. To account for such an uncertainty on the monomer properties and give error bars on the long-range coefficients, we have thus calculated a second set of coefficients (set B) by selecting literature values for the monomer moments. For Si, we have taken the Q_{20}^{Si} ab initio value of ref 25, evaluated at the CCSD(T) level with an aug-cc-pV5Z basis set. Static and dynamic polarizabilities of Si are those calculated in the present work (set A) since, up to our knowledge, the dynamic quantities are reported here for the first time. However, the accuracy of the static polarizabilities can be assessed by comparison with literature values, and our values obtained for both components α_{uu}^{Si} lie within less than 1% of ab initio values of ref 29 obtained at the CCSD(T) level with an aug-cc-pVQZ basis set extended to (17s, 12p, 4d, 3f, 2*g*). For OH, we have taken the Spelsberg[22] values for Q_{10}^{OH}, Q_{20}^{OH}, and $Q_{2\pm 2}^{OH}$. Furthermore, we have generated the dynamic polarizabilities from the pseudo-oscillator strengths and pseudo-energies tabulated by Spelsberg in ref 22 for ${}^{xx}\alpha_{lml'm'}^{\pm\pm}$ and ${}^{xy}\alpha_{lml'm'}^{\pm\mp}$. Those values were computed by means of single-excitation MRCI calculations (SE-MRCI) within the averaged coupled pair functional formalism (ACPF) and the basis set of ref 33.

IV. Interaction Coefficients

The long-range coefficients for the electrostatic, induction, and dispersion interactions have been evaluated for Si(^{3}P) + OH($X^2\Pi$) from the knowledge of the permanent multipole and static and dynamic polarizabilities of each monomer, discussed in section III. The long-range coefficients ${}^{ii'jj'}V_{nL_bM_aM_b}$ (see eqs 5, 9, and 12 of ref 9) are reported in the (LS) coupling case in Tables 4 and 5 for the electrostatic and polarization (induction plus dispersion) contributions, respectively, where i or i' stands for $|LSM_LM_S\rangle \equiv |M_L\rangle$ for Si(^{3}P) (since long-range matrix elements vanish unless $M'_S = M_S$ when spin−orbit interactions are neglected), and j or j' stands for $|\Lambda\Sigma\rangle \equiv |\Lambda\rangle$ for OH($X^2\Pi$) (long-range matrix elements vanish unless $\Sigma' = \Sigma$). One has to use eqs 4, 8, and 11 of ref 9 to get the related coefficients in the *JJ* coupling case, i.e., in the $|JM_J\rangle$ basis for Si and in the doubly degenerate $|\pm\Omega\rangle$ basis for OH. In this latter case, the $|\pm\Omega\rangle$ set of wave functions are directly obtained from those in the LS coupling case by the relations $|\pm\Omega\rangle = |\pm\Lambda \pm \Sigma\rangle$ or $|\pm\Omega\rangle = |\pm\Lambda \mp \Sigma\rangle$. The electrostatic coefficients have been tabulated for the dipole−quadrupole ($n = 4$) and quadrupole−quadrupole ($n = 5$) interactions, the dispersion coefficients for the dipole-induced−dipole-induced ($n = 6$) interactions and the induction coefficients for dipole−dipole-induced interaction ($n = 6$). Notice that the induction coefficients vanish for off-diagonal matrix elements $|\Lambda - \Lambda'| = 2$, due to the restriction given by $|\Lambda - \Lambda'| \le l_b$, where $l_b = 1$ for a dipole moment $Q_{l_bm_b}$.

To the best of our knowledge, no long-range coefficients have been determined for the Si + OH system up to now. This work is thus the first determination and no comparison is possible but estimated values of long-range coefficients for the dispersion and induction contributions can be retrieved when one considers state-averaged quantities (the electrostatic contribution cancels for state-averaged quantities). Indeed, in such a case, the long-range polarization energies take a form similar to that derived for closed-shell atom−diatom interacting species.[34,35] The dispersion energy for the dipole−induced dipole-induced case ($n = 6$) simplifies as

$$
E_{\mathrm{disp}}(R,\gamma) = -\frac{1}{R^6}[C_{6,\mathrm{disp}}^0 + C_{6,\mathrm{disp}}^2 P_2(\cos\gamma)] \tag{3}
$$

where the isotropic long-range coefficient written

$$
C_{6,\mathrm{disp}}^0 = \frac{3}{\pi}\int_0^\infty \bar{\alpha}_{\mathrm{OH}}(i\omega)\,\bar{\alpha}_{\mathrm{Si}}(i\omega)\,d\omega \approx \frac{3}{2}\frac{\eta_{\mathrm{OH}}\eta_{\mathrm{Si}}}{\eta_{\mathrm{OH}} + \eta_{\mathrm{Si}}}\bar{\alpha}_{\mathrm{OH}}\bar{\alpha}_{\mathrm{Si}} \tag{4}
$$

and the anistropic coefficient is

$$
C_{6,\mathrm{disp}}^2 = \frac{1}{\pi}\int_0^\infty \Delta\alpha_{\mathrm{OH}}(i\omega)\,\bar{\alpha}_{\mathrm{Si}}(i\omega)\,d\omega \approx \frac{1}{2}\frac{\eta_{\mathrm{OH}}\eta_{\mathrm{Si}}}{\eta_{\mathrm{OH}} + \eta_{\mathrm{Si}}}\Delta\alpha_{\mathrm{OH}}\bar{\alpha}_{\mathrm{Si}} \tag{5}
$$

On the right-hand side of eqs 4 and 5, the London approximation[36,37] is used to evaluate the dispersion coefficients, where η_i are the ionization energies of each species. The average static polarizabilities of Si and OH are given in Table 2, and the anisotropic polarizability of OH is here defined as $\Delta\alpha_{\mathrm{OH}} = {}^{xx}\alpha_{zz} - {}^1/_2[{}^{xx}\alpha_{xx} + {}^{xx}\alpha_{yy}]$. Using the values of Table 2, together with the London approximation and tabulated ionization energies[38] to evaluate the dispersion coefficients, we get $C_{6,\mathrm{disp}}^0 = 78.07/78.42$ au and $C_{6,\mathrm{disp}}^2 = 6.09/6.18$ au for the sets A/B. Since the state-averaged coefficients of eqs 4 and 5 are formally equivalent to those obtained by summing over diagonal matrix elements ($M_a = M_b = 0$) of the long-range dispersion coefficients ${}^{ii'jj'}V_{nL_bM_aM_b}$, we can retrieve state-averaged quantities from the tabulated values ${}^{ii'jj'}V_{6,000}$ and ${}^{ii'jj'}V_{6,200}$ of Table 5. The results obtained for the sets A/B, i.e., $C_{6,\mathrm{disp}}^0 = 86.13/85.97$ au, and $C_{6,\mathrm{disp}}^2 = 6.61/6.74$ au, are found to be in rather good agreement with the values yielded by the London approximation. The state-averaged induction energy for the dipole dipole-induced case ($n = 6$) takes a form similar to eq 3, with $C_{6,\mathrm{ind}}^0 = C_{6,\mathrm{ind}}^2 = \bar{\alpha}_{\mathrm{Si}}(Q_{10}^{\mathrm{OH}})^2$, and contribution of the quadrupole moment Q_{20}^{OH} cancels for state-averaged quantities. Using the dipole moment and static polarizabilities values of Tables 1 and 2, we get $C_{6,\mathrm{ind}}^0 = 16.17/15.68$ au for the sets A/B. The state-averaged coefficients retrieved from the tabulated coefficients ${}^{ii'jj'}V_{6,000}^{\mathrm{ind}}$ and ${}^{ii'jj'}V_{6,200}^{\mathrm{ind}}$ of Table 5 provide an identical value.

TABLE 4: Long-Range Non-Zero $^{ii'jj'}V_{4L_bM_aM_b}$ and $^{ii'jj'}V_{5L_bM_aM_b}$ Electrostatic Coefficients (in au) for the Si(^{3}P) + OH(X$^2\Pi$) Interaction

						$^{ii'jj'}V_4^{elec}$					$^{ii'jj'}V_5^{elec}$	
M_L	M'_L	$\Lambda\Lambda'$	M_a	M_b	L_b	set A	set B	M_a	M_b	L_b	set A	set B
±1	±1	±1 ± 1	0	0	1	−3.27	−3.24	0	0	2	−13.10	−13.11
±1	0	±1 ± 1	±1	0	1	3.27	3.24	±1	0	2	15.12	15.14
±1	∓1	±1 ± 1	±2	0	1	0.00	0.00	±2	0	2	−5.35	−5.35
0	±1	±1 ± 1	∓1	0	1	−3.27	−3.24	∓1	0	2	−15.12	−15.14
0	0	±1 ± 1	0	0	1	6.63	6.48	0	0	2	26.20	26.22
±1	±1	±1 ∓ 1						0	±2	2	12.49	12.18
±1	0	±1 ∓ 1						±1	±2	2	−14.42	−14.06
±1	∓1	±1 ∓ 1						±2	±2	2	5.10	4.97
0	±1	±1 ∓ 1						∓1	±2	2	14.42	14.06
0	0	±1 ∓ 1						0	±2	2	−24.99	−24.36

TABLE 5: Long-Range Non-Zero $^{ii'jj'}V_{6L_bM_aM_b}$ Dispersion and Induction Coefficients (in au) for the Si(^{3}P) + OH(X$^2\Pi$) Interaction

						$^{ii'jj'}V_6^{disp}$							$^{ii'jj'}V_6^{ind}$	
M_L	M'_L	$\Lambda\Lambda'$	M_a	M_b	L_b	set A	set B	M_L	M'_L	$\Lambda\Lambda'$	M_a	M_b	L_b	set A	set B
±1	±1	±1 ± 1	0	0	0	87.86	87.71	±1	±1	±1 ± 1	0	0	0	16.79	16.27
±1	±1	±1 ± 1	0	0	2	7.03	7.16	±1	±1	±1 ± 1	0	0	2	17.98	17.44
±1	0	±1 ± 1	±1	0	2	−0.48	−0.49	±1	0	±1 ± 1	±1	0	2	−2.09	−2.03
±1	∓1	±1 ± 1	±2	0	2	0.34	0.35	±1	∓1	±1 ± 1	±2	0	2	1.48	1.44
0	±1	±1 ± 1	∓1	0	2	0.48	0.49	0	±1	±1 ± 1	∓1	0	2	2.09	2.03
0	0	±1 ± 1	0	0	0	82.67	82.51	0	0	±1 ± 1	0	0	0	14.96	14.51
0	0	±1 ± 1	0	0	2	5.78	5.89	0	0	±1 ± 1	0	0	2	12.55	12.17
±1	±1	±1 ∓ 1	0	±2	2	5.089	4.195								
±1	0	±1 ∓ 1	±1	±2	2	−0.403	−0.342								
±1	∓1	±1 ∓ 1	±2	±2	2	0.285	0.242								
0	±1	±1 ∓ 1	∓1	±2	2	0.403	0.342								
0	0	±1 ∓ 1	0	±2	2	4.042	3.306								

The differences between the set A and set B coefficients reported in Tables 4 and 5 for the electrostatic and induction interactions result directly from the uncertainty in the multipole moments and static polarizabilities, and, in the present case, especially from the uncertainty on the quadrupole moment of OH. Indeed, the discrepancies are less than 1% between the monomer properties of sets A and B for Q_{20}^{Si}, Q_{10}^{OH}, and Q_{20}^{OH}, while they rise up to 3% for $Q_{2\pm2}^{OH}$. Similar discrepancies are observed on the related long-range V_4^{elec} (∼1%), V_5^{elec} (0.4%), and V_6^{ind} (3%) coefficients. The discrepancy is around 3% for the state-averaged coefficient $C_{6,ind}^0$. For the dispersion contribution, the discrepancies between the sets A and B are not so directly related to the averaged uncertainty on the dynamic polarizabilities of OH (dynamic polarizabilities $\alpha_{uu}^{Si}(i\omega)$ are identical in sets A and B). The uncertainties for $\alpha_{uu}^{OH}(i\omega)$ are within 7−9% on average (less than 1% for $\omega = 0$), and we attain an overall agreement of 2−4% for the diagonal ($M_b = \Lambda - \Lambda' = 0$) V_6^{disp} coefficients, while the agreement is around 10−20% for the nondiagonal ($M_b = \pm2$) V_6^{disp} coefficients.

V. Behavior of the Long-Range Multipolar Potentials

The full (doubly degenerate) 18 × 18 multipolar potential matrix is built up in the $|JM_J\rangle|\Lambda\Sigma\rangle$ coupled basis, where each matrix element is evaluated as a sum of electrostatic, induction, dispersion, and spin−orbit energies following:

$$E_{tot}^{JM_JJ'M'_J\Lambda\Sigma\Lambda'\Sigma'} = E_{elec}^{JM_JJ'M'_J\Lambda\Sigma\Lambda'\Sigma'} + E_{disp}^{JM_JJ'M'_J\Lambda\Sigma\Lambda'\Sigma'} + E_{ind}^{JM_JJ'M'_J\Lambda\Sigma\Lambda'\Sigma'} + E_{SO}^{JM_JJ'M'_J\Lambda\Sigma\Lambda'\Sigma'} \quad (6)$$

The spin−orbit contribution is zero for nondiagonal elements, and the nonzero diagonal matrix elements are written as a function of the fine structure splittings δ^{OH} and δ_J^{Si}. Sorting the 18 spin−orbit matrix elements in a descending order of energy from top to bottom shows the upper 9 states $|JM_J\rangle|\Lambda\Sigma\rangle$ correspond to the OH($^2\Pi_{1/2}$) doubly degenerate states $|\Lambda = \pm1, \Sigma = \mp^1/_2\rangle$ and the lower 9 states $|JM_J\rangle|\Lambda\Sigma\rangle$ correspond to the OH($^2\Pi_{3/2}$) doubly degenerate states $|\Lambda = \pm1, \Sigma = \pm^1/_2\rangle$. Then, within each group of 9 states, by sorting the $|JM_J\rangle$ atomic states in the energetic decreasing order, Si(^{3}P$_2$), Si(^{3}P$_1$), and Si(^{3}P$_0$), with M_J indices running from top to bottom as $M_J = J$ to $M_J = -J$, the upper 9 spin−orbit matrix elements are sorted as follows: $\{\delta_2^{Si} + \delta^{OH}, \delta_2^{Si} + \delta^{OH}, \delta_2^{Si} + \delta^{OH}, \delta_2^{Si} + \delta^{OH}, \delta_2^{Si} + \delta^{OH}, \delta_1^{Si} + \delta^{OH}, \delta_1^{Si} + \delta^{OH}, \delta_1^{Si} + \delta^{OH}, \delta^{OH}\}$, and the lower 9 matrix elements are sorted as $\{\delta_2^{Si}, \delta_2^{Si}, \delta_2^{Si}, \delta_2^{Si}, \delta_2^{Si}, \delta_1^{Si}, \delta_1^{Si}, \delta_1^{Si}, 0\}$. The experimental fine structure splitting values have been used in the present work: $\delta^{OH} = 139.7$ cm^{-1},[39] $\delta_1^{Si} = 77.115$ cm^{-1} and $\delta_2^{Si} = 223.157$ cm^{-1}.[38] The latter spin−orbit matrix elements can be used together with the tabulated values for the $^{ii'jj'}V_{nL_bM_aM_b}$ matrix elements to build up the multipolar potential matrix for Si(^{3}P) + OH(X$^2\Pi$).

Before discussing the results obtained for the full multipolar potentials, we first compare the long-range nonrelativistic potentials (neglecting the spin−orbit interaction) with ab initio PESs provided by supermolecular calculations. The ab initio potentials were evaluated at the CASSCF level to get size-consistent energies, which is crucial for behavior of the potentials at long range. As no dynamical correlation is considered in the CASSCF calculations, the resulting ab initio potentials must be compared with potentials including the electrostatic and induction contributions only (without dispersion). To this end, the multipolar (electrostatic+induction) potential matrix has been computed from the tabulated values $^{ii'jj'}V_{nL_bM_aM_b}$ of Tables 4 and 5, and subsequently diagonalized. The supermolecular calculations have been carried out within the C_{2v} symmetry group for the linear configurations ($\gamma = 0$

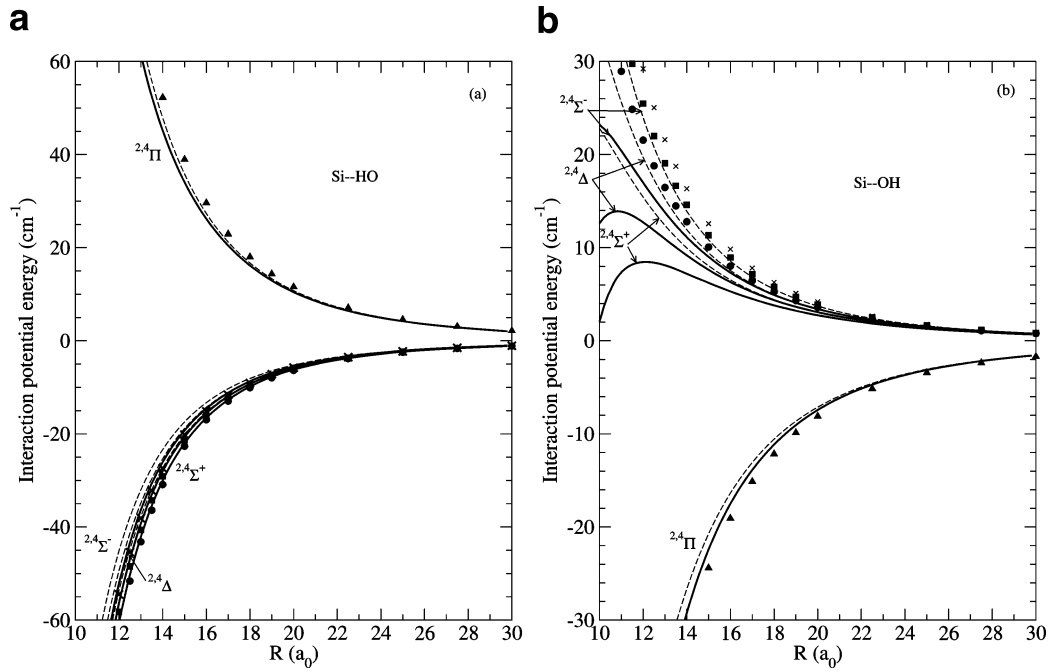

Figure 1. Full multipolar (continuous line) or electrostatic plus induction only (dashed line) potential energies (in cm^{-1}) for the eight degenerate (12 nondegenerate) nonrelativistic long-range Si(^{3}P) + OH($X^2\Pi$) states as a function of the intermolecular distance R (in bohr) for linear geometries of the complex at $\gamma = 0°$ (a) and $\gamma = 180°$ (b). In addition, ab initio supermolecular CASSCF values are shown for comparison: (a) $X^{2,4}A'(^{2,4}\Sigma^+)$ (circle), $2^{2,4}A' - 1^{2,4}A''(^{2,4}\Delta)$ (square), $2^{2,4}A''(^{2,4}\Sigma^-)$ (cross), $3^{2,4}A' - 3^{2,4}A''(^{2,4}\Pi)$ (triangle); (b) $(X^{2,4}A' - 1^{2,4}A''(^{2,4}\Pi)$ (square), $2^{2,4}A'(^{2,4}\Sigma^+)$ (circle), $3^{2,4}A' - 2^{2,4}A''(^{2,4}\Delta)$ (triangle), $3^{2,4}A''(^{2,4}\Sigma^-)$ (cross).

and 180°), and the C_s point group in other cases (Figure 2). The CASSCF calculations have been conducted for the doublet adiabatic states dissociating into Si(^{3}P) + OH($X^2\Pi$). At linear geometries, they correspond to the four states of $C_{\infty v}$ symmetry, $^2\Sigma^+$, $^2\Sigma^-$, $^2\Pi$, and $^2\Delta$, or to the six nondegenerate states $(1-3)^2A'$ and $(1-3)^2A''$ within the C_s symmetry group. Since exchange interaction is negligable, the doublet states are degenerate with their quartet counterparts $^4\Sigma^+$, $^4\Sigma^-$, $^4\Pi$, and $^4\Delta$ at long-range. The CASSCF calculations have been carried out with the full valence active space built up with 11 electrons distributed in 9 molecular orbitals, $(5\sigma-9\sigma, 2\pi-3\pi)$ corresponding to the (3s, 3p) shells of Si, (2s, 2p) shells of O, and 1s shell of H. The first six inner-shell orbitals were kept doubly occupied during the optimization, and a state-averaged procedure with equal weights for the 6 doublet states dissociating into Si(^{3}P) + OH($X^2\Pi$) has been employed. The same basis sets as employed for the monomer calculations were used, i.e., aug-cc-pVQZ for Si and aug-cc-pV5Z for O and H. The resulting energies have been corrected for the basis set superposition error using the Boys and Bernardi counterpoise method.[40] To this end, each substate component of the fragments Si(^{3}P) and OH($^2\Pi$) has been calculated within a full valence state-averaged CASSCF scheme, using the same symmetry group and the same basis set as employed for the SiOH molecular complex. The reference for the interaction energies has been chosen at a R value sufficiently large (200 bohr) such as the equality E(SiOH) = E(Si) + E(OH) is exactly satisfied for all states under study.

We present in Figures 1 and 2 the full multipolar potentials for the eight degenerate (12 nondegenerate) adiabatic states $^{2,4}\Sigma^+$, $^{2,4}\Sigma^-$, $^{2,4}\Pi$, and $^{2,4}\Delta$ dissociating into Si(^{3}P) + OH($X^2\Pi$) at linear geometries. The potentials are plotted as a function of the intermolecular distance R for $\gamma = 0°$ in Figure 1a (Si−HO collinear approach) and for $\gamma = 180°$ in Figure 1b (Si−OH collinear approach), as well as a function of the angle of approach γ at $R = 25$ bohr in Figure 2. As can be seen in Figure 1, when spin−orbit interactions are neglected, the $^{2,4}\Sigma^+$, $^{2,4}\Delta$,

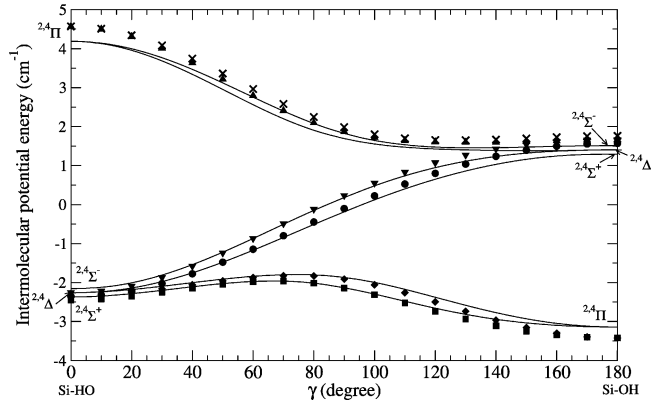

Figure 2. Full multipolar (continuous line) or electrostatic plus induction only (dashed line) potential energies (in cm^{-1}) for the eight degenerate (12 nondegenerate) nonrelativistic long-range Si(^{3}P) + OH($X^2\Pi$) states as a function of the OH bending angle, γ (in degree), at intermolecular distance $R = 25$ bohr. In addition, ab initio supermolecular CASSCF values are shown for comparison: $X^{2,4}A'(^{2,4}\Sigma^+ - ^{2,4}\Pi)$ (square), $2^{2,4}A'(^{2,4}\Delta - ^{2,4}\Sigma^+)$ (circle), $3^{2,4}A'$-$(^{2,4}\Pi - ^{2,4}\Delta)$ (triangle up), $1^{2,4}A''(^{2,4}\Delta - ^{2,4}\Pi)$ (diamond), $2^{2,4}A''$-$(^{2,4}\Sigma^- - ^{2,4}\Delta)$ (triangle down), $3^{2,4}A''(^{2,4}\Pi - ^{2,4}\Sigma^-)$ (cross).

and $^{2,4}\Sigma^-$ states form one group of quasi-degenerate states with an attractive behavior at $\gamma = 0°$ and with a repulsive behavior at $\gamma = 180°$, while the $^{2,4}\Pi$ states display opposite behavior. Such a feature had already been observed in the case of the C(^{3}P) + OH($X^2\Pi$) long-range interactions.[9] Furthermore, we compare in those figures the electrostatic + induction restricted multipolar energies with the supermolcular ab initio ones calculated at the CASSCF level. A good quantitative agreement is attained, the discrepancies being of the order of a few wavenumbers at the shortest intermolecular separations displayed in Figure 1. The same agreement is observed for all angles of approach, as can be seen in Figure 2. The remaining differences between the multipolar and ab initio potentials may

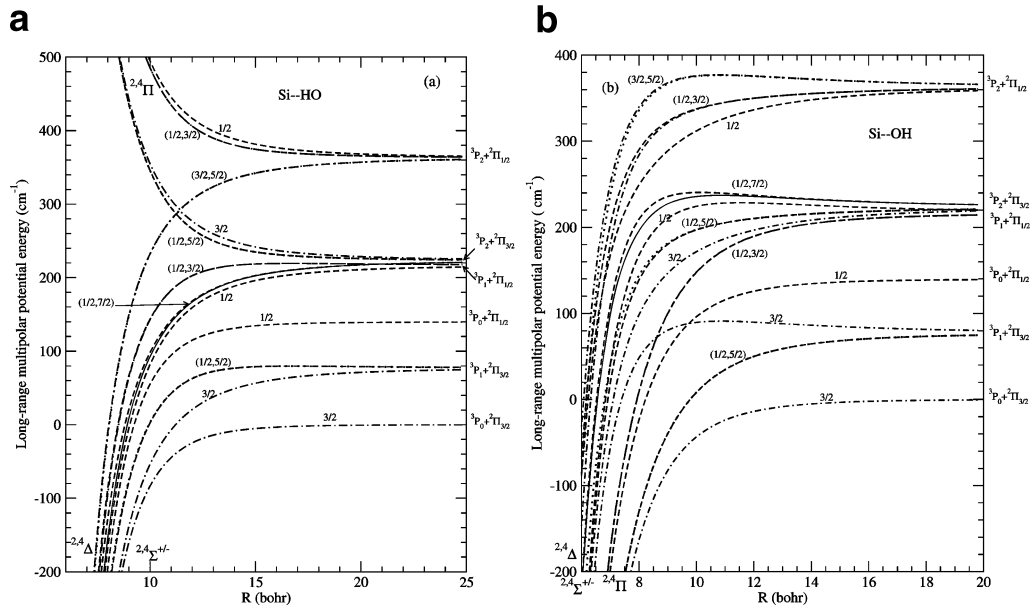

Figure 3. Full multipolar potential energies (in cm^{-1}) including monomer spin−orbit splittings for the 18 long-range Si(^{3}P) + OH(X$^2\Pi$) states as a function of the intermolecular distance R (in bohr) at $\gamma = 0°$ (a) and $\gamma = 180°$ (b). States are characterized by their Ω value: $^7/_2$ (continuous), $^5/_2$ (dotted), $^3/_2$ (dot-dashed), or $^1/_2$ (short dashed).

result from the use of different active spaces between the two calculations, from the static correlation included in the CASSCF calculations and/or from higher multipolar terms omitted in the multipolar expansion. To keep the calculations tractable, the active space employed in supermolecular calculations has been considerably reduced in regard to the active space used for the momoners properties. As a final comment, it is worth noting that the inclusion of the dispersion contribution changes drastically the feature of the excited states as observed in Figure 1b for the $^{2,4}\Sigma^+$, $^{2,4}\Delta$, and $^{2,4}\Sigma^-$ states and the Si−OH collinear approach. At short-range, the dispersion contribution compensates the repulsive electrostatic interaction, leading to the formation of small potential energy barriers around 10−12 bohr. For the Si−OH approach, the attractive dispersion effect is out of range of Figure 1a for the $^{2,4}\Pi$ states (presumably observable at shorter distances).

The full multipolar potentials including spin−orbit splittings, obtained by diagonalization of the full multipolar potential matrix, are displayed for the 18 spin−orbit states of Si(^{3}P) + OH(X$^2\Pi$) as a function of the intermolecular distance R for $\gamma = 0°$ in Figure 3a (Si−HO approach) and $\gamma = 180°$ in Figure 3b (Si−OH approach), as well as a function of the Jacobi angle γ at $R = 10$ bohr in Figure 4. In these figures, the states are labeled according to the value of the quantum number $\Omega_{tot} = M_J + \Lambda + \Sigma$, which is well-defined for linear geometries of the complex. Because the spin−orbit interaction for the Si(^{3}P) atom is much larger than for C(^{3}P), its effects are increased and will concern the higher temperature range (up to 600 K). Otherwise, the complexity and the general behavior of the potentials are similar to those of the C(^{3}P) + OH(X$^2\Pi$) case,[9] though the energetic order of the asymptotic spin−orbit states is different. Furthermore, the two asymptotes, $^3P_1 + {}^2\Pi_{1/2}$ and $^3P_2 + {}^2\Pi_{3/2}$ lie very close in energy, the former being lower than the latter, and that increases the density of states in this energy range. For both angles of approach, the relativistic potentials display several avoided crossings, and as a result of the dispersion contribution, potential energy barriers are observed for the linear Si−OH approach. At short distances, once the spin−orbit splitting becomes smaller than the interaction energies, the relativistic states converge toward the two groups

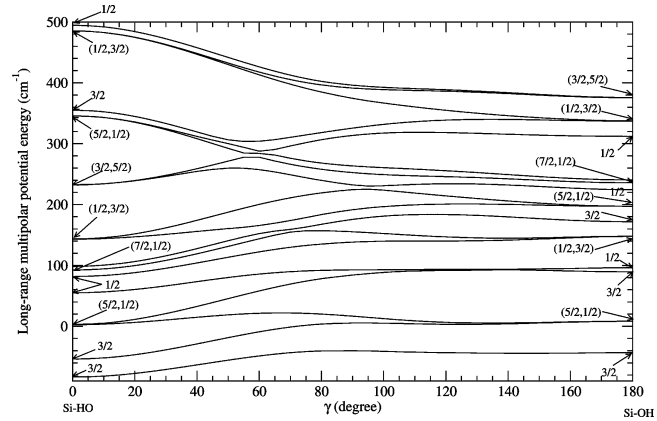

Figure 4. Full multipolar potential energies (in cm^{-1}) including monomer spin−orbit splittings for the 18 long-range Si(^{3}P) + OH(X$^2\Pi$) states as a function of the OH bending angle, γ (in degree), at intermolecular distance $R = 10$ bohr.

of nonrelativistic states $^{2S_{tot}+1}\Lambda_{tot}$ ($\Lambda_{tot} = M_L + \Lambda$ and $S_{tot} = S + \Sigma$) displayed in Figure 1. From the potentials displayed in Figure 4 at $R = 10$ bohr, we observe a quasi-isotropic potential for the ground state whereas the anisotropy is much more pronounced for the excited states. This was already the case for the ground nonrelativistic state (see Figure 2), but a slight preference now appears for the approach of the silicon atom on the hydrogen side of OH, while the oxygen side is preferred when spin−orbit splittings are neglected.

VI. Conclusion

We have calculated the long-range intermolecular potentials of the 18 spin−orbit states resulting from the interaction between two open-shell systems, Si(^{3}P) and OH(X$^2\Pi$). The diatomic OH has been kept fixed at its ground vibrational state averaged distance $\langle r \rangle_{v=0} = 1.865$ bohr. The long-range interaction potentials are thus two-dimensional potential energy surfaces (PESs) that depend on the intermolecular distance R and the angle γ between R and r. The potential matrix elements have been evaluated from the perturbation theory up to second order

using a two-center expansion of the Coulombic intermolecular potential operator with a diabatic basis product of unperturbed monomer electronic wave functions. A multipolar expansion of the potential is further expressed as a series of terms varying in R^{-n}. The determination of the expansion coefficients relies on the knowledge of monomer properties such as the permanent multipole moments, static and dynamic polarizabilities which have been carefully calculated or selected from literature values. The interaction potentials have been evaluated as a sum of electrostatic energies, which include the dipole−quadrupole (in R^{-4}) and quadrupole−quadrupole (in R^{-5}) interactions, as well as dispersion and induction energies, which include the dipole-induced−dipole-induced (dispersion) and dipole−dipole-induced (induction) interactions, i.e., limited to the terms varying in R^{-6}. The spin−orbit effects have been included by accounting for the experimental fine-structure splittings of the monomers. The diagonalization of the 18 × 18 full potential matrix generates the adiabatic long-range PESs. A comparison between present potentials and their ab initio counterparts obtained at the CASSCF level within a supermolecular formalism was made, and a good agreement between both approaches is observed.

Acknowledgment. B.B.H. acknowledges the support of the "Institut du Développement des Ressources en Informatique Scientifique" (IDRIS) in Orsay (France), of the UTINAM computer center and thanks the "Pole des Sciences Planétaires Bourgogne-Franche-Comté" for fruitful discussions. B.B.H. thanks Christopher Bender for English improvements.

References and Notes

(1) Gusdorf, A.; Pineau Des Forets, G.; Cabrit, S.; Flower, D. R. *A. & A.* **2008**, *490*, 695.
(2) Jiménez-Serra, I.; Martín-Pintado, J.; Caselli, P.; Viti, S.; Rodríguez-Franco, A. *Astrophys. J.* **2009**, *695*, 149.
(3) Gusdorf, A.; Cabrit, S.; Flower, D. R.; Pineau Des Forets, G. *A. & A.* **2008**, *482*, 809.
(4) Le Picard, S. D.; Canosa, A.; Pineau Des Forets, G.; Rebrion-Rowe, C.; Rowe, B. R. *A. & A.* **2001**, *372*, 1064.
(5) Gómez Martín, J. C.; Blitz, M. A.; Plane, J. M. C. *Phys. Chem. Chem. Phys.* **2009**, *11*, 671.
(6) Dayou, F.; Spielfiedel, A. *J. Chem. Phys.* **2003**, *119*, 4237.
(7) Le Picard, S. D.; Canosa, A.; Reignier, D.; Stoecklin, T. *Phys. Chem. Chem. Phys.* **2002**, *4*, 3659.
(8) McCarthy, M. C.; Tamassia, F.; Woon, D. E.; Thaddeus, P. *J. Chem. Phys.* **2008**, *129*, 184301.
(9) Bussery-Honvault, B.; Dayou, F.; Zanchet, A. *J. Chem. Phys.* **2008**, *129*, 234302.
(10) Zanchet, A.; Bussery-Honvault, B.; Honvault, P. *J. Phys. Chem. A* **2006**, *110*, 12017.
(11) Zanchet, A.; Halvick, Ph.; Rayez, J. C.; Bussery-; Honvault, B.; Honvault, P. *J. Chem. Phys.* **2007**, *126*, 184308.
(12) Zanchet, A.; Halvick, Ph.; Bussery-Honvault, B.; Honvault, P. *J. Chem. Phys.* **2008**, *128*, 204301.
(13) Bulut, N.; Zanchet, A.; Honvault, P.; Bussery-Honvault, B.; Banares, L. *J. Chem. Phys.* **2009**, *130*, 194303.
(14) Schenewerk, M. S.; Snyder, L. E.; Hjalmarson, Å. *Astrophys. J.* **1986**, *303*, L71.
(15) Lee, S.-H.; Liu, K. I. In *Advances in Molecular Beam Research and Applications*; Campargue, R., Ed.; Springer-Verlag: Berlin, 2000.
(16) Casavecchia, P. *Rep. Prog. Phys.* **2000**, *63*, 355.
(17) Smith, I. W. M.; Herbst, E.; Chang, Q. *MNRAS* **2004**, *350*, 323.
(18) Carty, D.; Goddard, A.; Kohler, S. P. K.; Sims, I. R.; Smith, I. W. M. *J. Phys. Chem. A* **2006**, *110*, 3101.
(19) Graff, M. M.; Wagner, A. F. *J. Chem. Phys.* **1990**, *92*, 2423. Graff, M. M. *ApJ* **1989**, *339*, 239.
(20) *DALTON, a molecular electronic structure program*, Release 2.0; 2005; see http://www.kjemi.uio.no/software/dalton/dalton.html.
(21) Peterson, K. I.; Fraser, G. T.; Klemperer, W. *Can. J. Phys.* **1984**, *62*, 1502.
(22) Spelsberg, D. *J. Chem. Phys.* **1999**, *111*, 9625.
(23) Wormer, P. E. S.; Klos, J. A.; Groenenboom, G. C.; Van der Avoird, A. *J. Chem. Phys.* **2005**, *122*, 244325.
(24) Nelson, D. D.; Schiffman, A.; Nesbitt, D. J.; Orlando, J. J.; Burkholder, J. B. *J. Chem. Phys.* **1990**, *93*, 7003.
(25) Gutsev, G. L.; Jena, P.; Bartlett, R. J. *Chem. Phys. Lett.* **1998**, *291*, 547.
(26) Andersson, K.; Sadlej, A. J. *Phys. Rev.* **1992**, *46*, 2356.
(27) Fowler, P. W.; Jørgensen, P.; Olsen, J. *J. Chem. Phys.* **1990**, *93*, 7256.
(28) Langhoff, P. W.; Karplus, M. *J. Chem. Phys.* **1970**, *53*, 233.
(29) Thierfelder, C.; Assadollahzadeh, B.; Schwerdtfeger, P.; Schäfer, S.; Schäfer, R. *Phys. Rev. A* **2008**, *78*, 52506.
(30) Lupinetti, C.; Thakkar, A. J. *J. Chem. Phys.* **2005**, *122*, 44301.
(31) Karna, S. P. *J. Chem. Phys.* **1996**, *104*, 6590.
(32) Maroulis, G.; Pouchan, C. *J. Phys. B: At. Mol. Opt. Phys.* **2003**, *36*, 2011.
(33) Spelsberg, D.; Meyer, W. *J. Chem. Phys.* **1998**, *108*, 1532.
(34) Langhoff, P. W.; Gordon, R. G.; Karplus, M. *J. Chem. Phys.* **1971**, *55*, 2126.
(35) Nielson, G. C.; Parker, G. A.; Pack, R. T. *J. Chem. Phys.* **1976**, *64*, 2055.
(36) London, F. *Z. Physik. Chem.* **1930**, *B11*, 222.
(37) Buckingam, A. D. *Adv. Chem. Phys.* **1967**, *12*, 107.
(38) National Institute of Standards and Technology, http://www.nist-.gov/.
(39) Chase, M. W.; Curnutt, J. L.; Downey, J. R.; McDonald, R. A.; Syverud, A. N.; Valenzuela, E. A. *J. Phys. Chem. Ref. Data* **1982**, *11*, 695.
(40) Boys, S. F.; Bernardi, F. *Mol. Phys.* **1970**, *19*, 553.

JP905090X